Nanocolloid Cake Properties Determined from Step-Up Pressure Filtration with Single-Stage Reduction in Filtration Area

Eiji Iritani, Nobuyuki Katagiri, and Ryota Nakajima
Dept. of Chemical Engineering, Nagoya University, Furo-cho, Chikusa-ku, Nagoya 464-8603, Japan

Kuo-Jen Hwang and Tung-Wen Cheng
Dept. of Chemical and Materials Engineering, Tamkang University, Tamsui, New Taipei City 25137, Taiwan

DOI 10.1002/aic.14967
Published online August 1, 2015 in Wiley Online Library (wileyonlinelibrary.com)

A sophisticated method was developed for evaluating simultaneously and accurately both the average specific resistance and average porosity of the filter cake formed in unstirred dead-end ultrafiltration of nanocolloids such as protein solution and nanosilica sol. In the method, a step-up pressure filtration test was conducted by using a filter with a single-stage reduction in the effective filtration area. The influence of the pressure drop across the cake on not only the average specific cake resistance but also on the average cake porosity of highly compressible filter cake was evaluated using only flux decline data in one dead-end filtration test, taking advantage of the decrease in the cake thickness caused by the pressure increase. As a result, the cake properties were easily determined for a variety of nanocolloids. Constant pressure dead-end ultrafiltration data obtained under various pressures and concentrations were well evaluated based on the method proposed. © 2015 American Institute of Chemical Engineers *AIChE J*, 61: 4426–4436, 2015
Keywords: step-up pressure filtration, ultrafiltration, cake property, nanocolloid, filtration area

Introduction

The filtration process of protein solutions and nanocolloids using ultrafiltration membranes plays an increasingly important and indispensable role in widely diversified fields ranging from industry to environmental protection. In membrane filtration, membrane fouling is a critical problem leading to the degradation of ultrafiltration performance and causes a dramatic flux decline during the process due to a significant increase in the filtration resistance. There exist several factors affecting membrane fouling, for example, cake formation,[1–8] pore blocking and/or pore constriction,[9,10] solute adsorption,[11,12] and concentration polarization.[13,14] Among them, the impact of the filter cake on the flux decline behavior in ultrafiltration is still not fully understood in spite of its importance. The average specific cake resistance α_{av} is one of the most important factors influencing cake properties and is a measure of the filterability. The average cake porosity ε_{av} is also a highly important factor which is closely related to the cake structure, and it has a profound influence on the filterability. Therefore, it is just as essential to evaluate both α_{av} and ε_{av} of the filter cake formed on the membrane surface from dead-end filtration tests also for ultrafiltration[3,15–18] as it is for traditional cake filtration of particulate suspension.[19–22] Especially, an understanding of pressure dependences of α_{av} and ε_{av} of the highly compressible filter cake serves as a basis for the operation control of ultrafilter equipment. The dependences of α_{av} and ε_{av} on the pressure drop Δp_c across the cake obtained from the filtration data are closely related to the compression-permeability data representing the local specific cake resistance α and local cake porosity ε as functions of the solute compressive pressure p_s, leading to the understanding of the internal structure of the filter cake.[3,23–31] Among them, Iritani et al.[3] developed the method for evaluating the internal cake structure based on pressure dependences of α_{av} and ε_{av} obtained from filtration data. More recently, Bouchoux et al.[31] evaluated the concentration dependence of the permeability, which is closely related the average specific cake resistance, from the filtration data when the concentration dependence of the osmotic pressure is known from the osmotic pressure measurements.

The value of α_{av} corresponding to the applied filtration pressure p can be obtained based on the compressible cake filtration model[32–35] from the variation of filtration rate with time measured in a constant pressure filtration experiment. In typical constant pressure filtration, the pressure drop Δp_c across the cake is nearly identical to the applied pressure p throughout the period of filtration since the filter medium resistance is generally negligible compared to the cake resistance. Accordingly, the relation between α_{av} and Δp_c can be basically determined from several constant pressure filtration experiments accomplished under different applied pressure conditions.

This relation can be obtained from monitoring the pressure rising behaviors with time by conducting a constant rate filtration experiment in which the filtration rate is maintained

Correspondence concerning this article should be addressed to E. Iritani at iritani@nuce.nagoya-u.ac.jp.

Table 1. Properties of Selected Proteins

Protein	Molecular Weight (kDa)	Isoelectric Point	Partial Specific Volume (cm^3/g)
BSA	67	5.1	0.733
Lysozyme	14.3	11.0	0.726
Myoglobin	17.8	7.0	0.741
Hemoglobin	64.5	6.8	0.746
γ-Globulin	159	5.86–6.70	0.730

constant.[36] Not only α_{av} but also ε_{av} (i.e., the ratio m of the mass of wet to mass of dry cake) vary with the increase in the applied pressure with time in the case of the compressible filter cake deposited during constant rate filtration. However, in this case, approximate data analysis is generally performed by ignoring the variation of ε_{av} with Δp_c. When the time variations of the applied filtration pressure and filtration rate can be measured, the pressure dependence of α_{av} is evaluated also from a variable pressure filtration experiment in which both pressure and filtration rate are time dependent.[37] Step-up pressure filtration[38] in which the applied pressure is increased incrementally is considered as a type of variable pressure filtration, but it can also offer information about the pressure dependence of α_{av} more easily than normal variable pressure filtration.

In the single constant pressure filtration method developed recently,[39,40] the relation between α_{av} and Δp_c can be evaluated only from the flux decline data in a single filtration experiment by using a filter medium with an extremely high hydraulic resistance compared to the cake resistance even in the initial observable period of filtration. To acquire the data over a much wider range of pressures, the single step-up pressure filtration experiment was conducted by increasing the pressure in stages during the course of filtration.[41]

It is essential to obtain the average cake porosity ε_{av} as a function of the pressure drop Δp_c across the cake to evaluate a more accurate α_{av} and to comprehend the structure of compressible filter cake formed on the membrane surface during filtration. While ε_{av} is exclusively determined by directly weighing the filter cake before and after the cake dries, visual determination of the end of filtration often leads to erroneous values because of the indistinct interface between the cake surface and the slurry. The cake porosity can be evaluated by measuring the distributions of hydraulic pressure and electrical resistance within the filter cake.[42,43]

The cake porosity can be relatively easily evaluated based on an abrupt decrease in the flux occurring by using a filter causing a sudden reduction in the cake surface area in the course of filtration.[44,45] The method is successfully applied not only to filtration of particulate suspension[44,45] but also to ultrafiltration of protein solution in which it is quite difficult to measure the cake porosity ε_{av}.[3,46] While several constant pressure filtration experiments are required to obtain the relation between ε_{av} and Δp_c, the measurement of hydraulic pressure distribution within the filter cake in a step-up pressure filtration experiment allows us to evaluate the pressure dependence of ε_{av}.[38] However, the measurement of the hydraulic pressure is quite laborious and requires much skill. As an alternative, a filter in which the filtration area decreases with the distance from the filter medium in stages is employed in a step-up pressure filtration experiment to readily evaluate the relationship of ε_{av} to Δp_c.[47] But, a sudden reduction in the cake surface area promotes the unfavorable consolidation of the preformed filter cake when the cake is highly compressible.

In the previous paper,[48] a method has been developed for evaluating both α_{av} and ε_{av} as functions of Δp_c from only two dead-end ultrafiltration experiments using a filter with a reduction in the filtration area. Although the method is quite effective in determining the cake properties, two data points of ε_{av} vs. Δp_c are insufficient to obtain the accurate relation between ε_{av} and Δp_c. To our knowledge a filtration testing method remains to be developed for simultaneously and easily obtaining the data of α_{av} and ε_{av} vs. Δp_c from only one experiment despite a large number of filtration studies.

In this article, a method is developed for more rigorously evaluating both the average specific resistance α_{av} and average porosity ε_{av} of highly compressible filter cake formed on the membrane surface in dead-end ultrafiltration of nanocolloids over a wide range of pressures Δp_c from only one experiment. The method is based on step-up pressure filtration using a filter with a single-stage reduction in the filtration area. After the cake surface reaches the position where the filtration area is reduced, the cake thickness decreases due to the compressibility of filter cake by a sudden increase in the applied filtration pressure. Consequently, a sudden reduction effect in the filtration area is available more than once by conducting step-up pressure filtration. The relation between α_{av} and Δp_c can be evaluated from a gradual decline behavior in the flux during each constant pressure filtration period before the cake surface reaches the position where the filtration area is reduced. The relation between ε_{av} and Δp_c can be determined from an abrupt decline in the flux occurring when the cake surface reaches the position where the filtration area is reduced at each applied filtration pressure. The availability of the method developed is confirmed by applying it to a variety of nanocolloids and by examining the effect of the solution environment such as pH and salt concentration and the colloid concentration.

Experimental

Materials

The proteins employed in the experiments were bovine serum albumin (BSA) (Fraction V, Sigma-Aldrich Japan), lysozyme from chicken egg white (Sigma-Aldrich Japan), myoglobin from horse heart (Sigma-Aldrich Japan), hemoglobin from bovine blood (Sigma-Aldrich), and γ-globulin from bovine plasma (Sigma-Aldrich). Table 1 lists the properties of these proteins such as the molecular weight, the isoelectric point (pI), and the partial specific volume of solute, which is considered to be equal to the reciprocal of the density of solute.[41,46,49–52] The solutions of silica sol (Snowtex (ST), Nissan Chemical Industries) with four different mean particle sizes were also used in the experiments. The mean specific surface area sizes d_s of ST-XS, ST-20, ST-20L, and ST-ZL were calculated from the particle-size distributions measured by a dynamic light scattering (DLS) photometer (DLS-8000, Otsuka Electronics), and they were 4.8, 13.3, 55.3, and 99.7 nm, respectively. The densities ρ_s of the particles were 2270, 2200, 2240, and 2230 kg/m^3, respectively.

Dilute aqueous solutions were prepared by dispersing preweighed quantities of the powder or solutions in ultrapure, deionized water (resistivity of at least 18 MΩ cm) produced by purifying tap water through ultrapure water systems equipped both with Elix-UV20 and with Milli-Q Advantage (Bio-POD) for laboratory use (Millipore). In the preparation of protein solutions, the solution pH was adjusted to a desired value according to protein by adding a small amount of 0.1 M

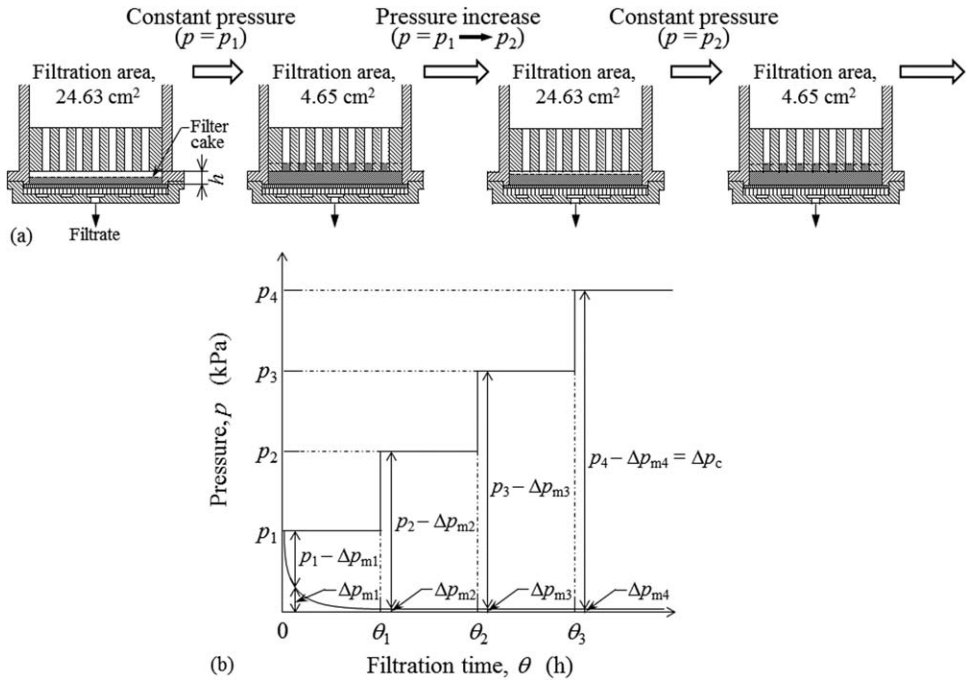

Figure 1. Mechanism of filtration process developed in this research.

(a) Schematic diagram representing growth of filter cake and (b) schematic diagram representing the relation between applied filtration pressure and filtration time.

NaOH or HCl solutions. But, in the case of γ-globulin, the solution pH was adjusted by using 10 mM phosphate buffer solution to prevent protein precipitation. In some experiments the ionic strength of BSA solution varied by adding NaCl (NaCl concentrations $C_s = 100$ and 200 mol/m^3). The concentrations by weight fraction of the protein and silica sol were adjusted to 0.005 and 0.01, respectively. In some experiments, the solutions of ST-XS were prepared at the different concentrations ranging from 0.01 to 0.1.

Experimental apparatus and technique

The experiments were conducted in the dead-end filtration mode by using an unstirred batch filtration cell with an effective area of 24.63 cm^2, which was exactly the same as the one used in the previous study.[48] The filter was structurally designed by equipping the orifice structure at the distance h of 0.43 mm from the membrane surface, as illustrated in Figure 1a, so that the average cake porosity ε_{av} was evaluated only from the flux decline behaviors. Consequently, once the cake surface grows to the position of the orifice, the effective filtration area is abruptly reduced from the original value (24.63 cm^2) to 4.65 cm^2 as shown in the figure.

In the step-up pressure filtration proposed in this research, the pressure was sequentially increased as shown in Figure 1b by adjusting the applied filtration pressure p automatically using by a computer-driven electronic pressure regulator with the application of compressed gas, where θ is the filtration time and Δp_m is the liquid pressure drop across the membrane. Initially, constant pressure filtration started at the pressure p_1. Once the cake surface reached the orifice, the surface area of the filter cake was substantially decreased to 4.65 cm^2. Shortly afterward, the pressure was jumped straight to p_2 and constant pressure filtration was continued at that pressure. The moment the pressure was increased, the cake thickness decreased due to the cake compression arising from the increase in the pressure drop Δp_c across the cake. As a result, the cake recovered the original surface area of 24.63 cm^2. However, as filtration progressed, the cake surface reached the orifice once again and thus the cake surface area was substantially reduced. In a similar way, the pressure was sequentially increased to p_4 through p_3, as shown in Figure 1b, and step-up pressure filtration was conducted. As a consequence, the phenomenon of sudden decrease in the filtration area was available more than once. Asymmetric regenerated cellulose ultrafiltration membranes (Millipore) with nominal molecular weight cut-offs of 1, 3, and 10 kDa were employed depending on the solute size to ensure the complete rejection of solutes.

The filtrate was accumulated in a reservoir placed on an electronic balance (Shimadzu) connected to a personal computer to collect and record filtrate mass vs. filtration time data during a filtration run. The weights were converted to volumes with the use of density correlations to obtain the variation with time of the cumulative filtrate volume v per unit effective membrane area and thus the dependences of the filtration rate ($dv/d\theta$) on v and θ.

To confirm the validity and availability of the step-up pressure filtration tests developed in this research, several constant pressure dead-end filtration experiments of BSA solution were conducted under various pressures by using the same filter and membrane as that used in step-up pressure filtration tests. In addition, several constant pressure filtration experiments of nanosilica sol were carried out under various pressures and concentrations.

Results and Discussion

Time variation of filtration rate

A method has been developed for determining the dependence of the average specific cake resistance α_{av} and average cake porosity ε_{av} on the effective pressure drop Δp_c across the filter cake only from the measurement of the time variation of the filtration rate measured in just one filtration test. Figure 2

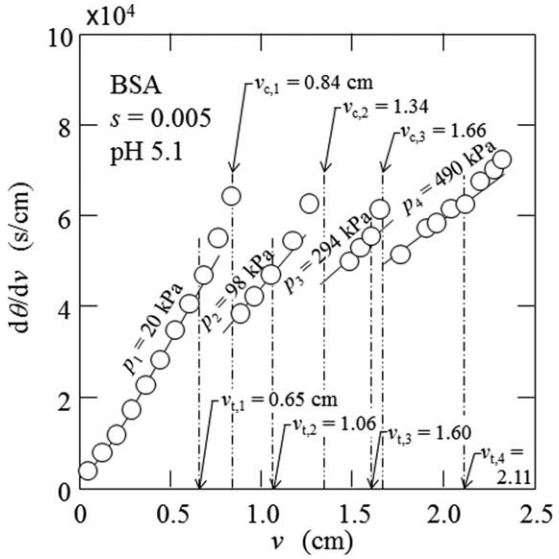

Figure 2. Relation between reciprocal filtration rate and filtrate volume per unit effective membrane area in ultrafiltration of BSA solution with concentration of 0.005 and pH 5.1.

illustrates the time variation of the filtration rate plotted in the form of the reciprocal filtration rate ($d\theta/dv$), which serves as a measure of the total filtration resistance, vs. the cumulative filtrate volume v per unit effective membrane area. Plots should show a straight line in constant pressure filtration in which the membrane resistance is negligible compared to the cake resistance on the basis of the Ruth cake filtration theory.[53]

The figure shows typical data obtained in step-up pressure filtration of BSA solution prepared at the solute mass fraction s of 0.005 and pH 5.1. The experiment was started with an initial constant pressure p_1 of 20 kPa to obtain the variation of α_{av} over the relatively small Δp_c range. Initially, the plots are very slightly concave upward because of the variation of α_{av} with Δp_c, and then tend to approach a linear relationship. However, $d\theta/dv$ undergoes a more rapid increase with v once v is beyond a critical value $v_{t,1}$ (= 0.65 cm). This is because the cake surface reaches the position where the inner cross-sectional area of the cell cylinder is reduced abruptly, as shown in Figure 1a.[3,44–46] As a consequence, the apparent filtration rate $dv/d\theta$ dramatically drops off due to a substantial decrease in the surface area of the growing filter cake.

After the rapid increase in $d\theta/dv$ is detected, the applied pressure is instantaneously increased to the second pressure p_2 of 98 kPa at the transition value $v_{c,1}$ (= 0.84 cm) and is thereafter maintained constant. At the instant that the pressure increases, $d\theta/dv$ decreases extremely, and then the plots immediately show a new linear relationship. However, after v reaches a critical value $v_{t,2}$ (= 1.06 cm), $d\theta/dv$ begins to deviate from this linearity. This intriguing behavior can be readily explained by the decrease in the cake thickness caused by the cake compressibility. The moment the pressure p is increased, the cake thickness L decreases below the distance h from the membrane surface to the position where the filtration area is reduced, as shown in Figure 1a. As a consequence, the cake surface area becomes equal to the membrane area again. At this time the plots show almost a linear relationship because the pressure drop p_m across the filter medium becomes negligibly small compared to the applied pressure p, influenced by both the continuing cake growth and the increased pressure p. Thereafter, as soon as the cake thickness becomes equal to h, $d\theta/dv$ increases abruptly. In a similar way, the applied pressure was increased to 294 and 490 kPa sequentially with the real-time monitoring of the filtration rate changing with time. The results exhibit a similar tendency to the case for 98 kPa. Consequently, the every time the pressure is increased in these cases, the cake recovers the original filtration area equivalent to the filter medium area.

The compressible cake filtration model is employed to analyze the properties of compressible filter cake in ultrafiltration of nanocolloids.[3,15–18] It is implicitly assumed in the model that all the colloidal particles convected toward the membrane accumulate on the surface as a filter cake because the experiments are conducted in the unstirred dead-end mode.[17] The cake growth occurring with the progress of filtration brings about the increase in the hydraulic resistance to the filtrate flow and thus the filtration rate declines with time.

Determination of α_{av} and ε_{av} from experimental data

On the basis of the compressible cake filtration model, the apparent liquid velocity u relative to solutes in the cake at distance ω from the membrane may be given in[41,54,55]

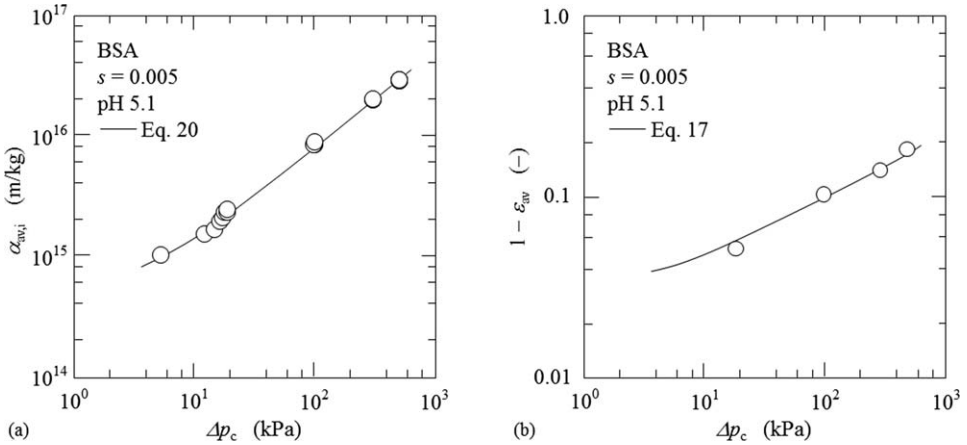

Figure 3. Pressure dependence of cake properties obtained in dead-end ultrafiltration of BSA solution with concentration of 0.005 and pH 5.1.

(a) Pressure dependence of infinite average specific cake resistance and (b) pressure dependence of average cake solidosity.

$$u=\frac{1}{\mu\rho_s\alpha}\cdot\frac{\partial p_L}{\partial\omega}=-\frac{1}{\mu\rho_s\alpha}\cdot\frac{\partial p_s}{\partial\omega} \tag{1}$$

where ω is the net solute volume per unit membrane area lying from the membrane up to an arbitrary position in the cake, μ is the viscosity of the filtrate, ρ_s is the density of solutes, and p_L is the local hydraulic pressure. While the concept of the solute compressive pressure p_s in the cake is used in the cake filtration model adopted in this article, p_s is strictly equivalent to the osmotic pressure Π in the polarized layer in the osmotic pressure model, as demonstrated by Jönsson and Jönsson,[56] Elimelech et al.,[57] and Bouchoux et al.[31] On the assumption that u remains constant throughout the entire cake at any instant in filtration of dilute colloids,[58] Eq. 1 is integrated from $\omega = 0$ to ω_0 and $p_s = \Delta p_c$ to 0 to give

$$u_1=\frac{dv}{d\theta}=\frac{\Delta p_c}{\mu\rho_s\omega_0\alpha_{av}} \tag{2}$$

where u_1 is the filtration rate, ω_0 is the net solute volume of the entire cake per unit membrane area, and α_{av} is given as[19]

$$\alpha_{av}=\frac{\Delta p_c}{\int_0^{\Delta p_c}\frac{1}{\alpha}dp_s} \tag{3}$$

In the cake filtration model used in unstirred dead-end filtration, it is implicitly assumed that all solutes convected toward the membrane accumulate in the cake.[3] On the basis of the material balance, it is convenient to transform Eq. 2 from ω_0 to v to give[40]

$$\frac{1}{u_1}=\frac{d\theta}{dv}=\frac{\mu\alpha_{av}\rho s}{\Delta p_c(1-ms)}v \tag{4}$$

where s is the mass fraction of solutes in colloids. In the above equation, the ratio m of the mass of wet to mass of dry cake is related to ε_{av} by the equation[20]

$$m=1+\frac{\rho\varepsilon_{av}}{\rho_s(1-\varepsilon_{av})} \tag{5}$$

where ρ is the density of filtrate. In Eq. 4, the pressure drop Δp_c across the filter cake is described by

$$\Delta p_c=p-\Delta p_m=p-\mu R_m u_1 \tag{6}$$

With the aid of Eq. 6, Eq. 4 is rewritten as[40,48,59]

$$\frac{1}{u_1}=\frac{d\theta}{dv}=\frac{\mu\alpha_{av}\rho s}{p(1-ms)}v+\frac{\mu R_m}{p} \tag{7}$$

where R_m is the membrane resistance. In Eqs. 6 and 7, R_m is given by[41]

$$R_m=\frac{p_1}{\mu}\left(\frac{d\theta}{dv}\right)_m \tag{8}$$

where $(d\theta/dv)_m$ is the reciprocal filtration rate at the start of filtration. Eqs. 7 and 6 combined with Eq. 8, respectively, lead to

$$\frac{1}{u_1}=\frac{d\theta}{dv}=\frac{\mu\alpha_{av}\rho s}{p(1-ms)}v+\frac{p_1}{p}\left(\frac{d\theta}{dv}\right)_m \tag{9}$$

$$\Delta p_c=p-\frac{(d\theta/dv)_m}{(d\theta/dv)}p_1 \tag{10}$$

Consequently, the relationship between $\alpha_{av}/(1 - ms)$ and Δp_c can be readily evaluated from the measurements of $d\theta/dv$ vs. v with the use of Eqs. 9 and 10.[39] It is, therefore, necessary to acquire the relation between m (i.e., ε_{av}) and Δp_c to accurately obtain the dependence of α_{av} on Δp_c. In case that the term $(1 - ms)$ in Eq. 9 is approximated by unity, Eq. 9 reduces to

$$\frac{1}{u_1}=\frac{d\theta}{dv}=\frac{\mu\alpha_{av}\rho s}{p}v+\frac{p_1}{p}\left(\frac{d\theta}{dv}\right)_m \tag{11}$$

In this case, the dependence of α_{av} on Δp_c can be obtained from Eqs. 10 and 11 without the information of the relation between m (or ε_{av}) and Δp_c.

The dependence of m (or ε_{av}) on Δp_c can be evaluated by using the value of v_t obtained at each pressure. As the total mass of colloid filtered is placed equal to the sum of the mass of wet cake and the mass of filtrate in unstirred dead-end filtration, an overall mass balance may be written as

$$\frac{\rho_s h(1-\varepsilon_{av})}{s}=\{\rho_s h(1-\varepsilon_{av})+\rho h\varepsilon_{av}\}+\rho v_t \tag{12}$$

Solving for ε_{av} results in[3]

$$\varepsilon_{av}=\frac{\rho_s h(1-s)-\rho s v_t}{\rho_s h(1-s)+\rho s h} \tag{13}$$

Having v_t vs. Δp_c data, one can derive the relationship between ε_{av} and Δp_c from the above equation. As a result, the dependence of α_{av} on Δp_c can be obtained from Eqs. 9 and 10 as described in the next section since ε_{av} (or m) vs. Δp_c is known.

Dependence of α_{av} and ε_{av} on Δp_c

In the particulate filter cake exhibiting compressible behaviors, both the average specific cake resistance α_{av} and average cake porosity ε_{av} are largely affected by the pressure drop Δp_c across the filter cake.[43–45] It becomes quite important to examine the cake compressibility also in dead-end ultrafiltration of nanocolloids.[3,4,15,46]

There exist several empirical expressions to relate α_{av} and ε_{av} to Δp_c. Over the relatively high Δp_c range, α_{av} and the average cake solidosity $(1 - \varepsilon_{av})$ representing the volume fraction of solids in the filter cake are expressed by unique power functions of Δp_c as[20,60]

$$\alpha_{av}=\alpha_1\Delta p_c{}^{n_1} \tag{14}$$

$$1-\varepsilon_{av}=(1-\varepsilon_1)\Delta p_c{}^{\beta_1} \tag{15}$$

where α_1, n_1, ε_1, and β_1 are the empirical constants. However, Eqs. 14 and 15 are not applicable to the relatively low Δp_c region. In the previous paper,[48] it was found that the following empirical equations with three fitting parameters for each property can be utilized to fit experimental data over a wide range of Δp_c

$$\alpha_{av}=\alpha_2\left(1+\frac{\Delta p_c}{p_a}\right)^{n_2} \tag{16}$$

$$1-\varepsilon_{av}=(1-\varepsilon_2)\left(1+\frac{\Delta p_c}{p_a}\right)^{\beta_2} \tag{17}$$

where α_2, p_a, n_2, ε_2, and β_2 are empirical constants. Of particular note is that the same parameter p_a in both Eqs. 16 and 17 is used to describe behaviors in the relatively low Δp_c range, as is the case in equations presented by Tiller and Lue.[61]

The quantity $\alpha_{av,i}$ is defined by

$$\alpha_{av,i} = \frac{\alpha_{av}}{1 - ms} \tag{18}$$

In the infinitely diluted colloid ($s = 0$), $\alpha_{av,i}$ is identical to α_{av}. Thus, $\alpha_{av,i}$ is named as the infinite average specific cake resistance.[62,63] Substituting Eq. 18 into Eq. 9 yields

$$\frac{1}{u_1} = \frac{d\theta}{dv} = \frac{\mu \alpha_{av,i} \rho s}{p} v + \frac{p_1}{p} \left(\frac{d\theta}{dv} \right)_m \tag{19}$$

The specific resistance $\alpha_{av,i}$ can be approximately represented by the empirical power law equation, which is similar to Eq. 16, in the form

$$\alpha_{av,i} = \alpha_3 \left(1 + \frac{\Delta p_c}{p_{a1}} \right)^{n_3} \tag{20}$$

where α_3, p_{a1}, and n_3 are empirical constants.

In Figure 3, $\alpha_{av,i}$ and $(1 - \varepsilon_{av})$ are logarithmically plotted against Δp_c, based on the data shown in Figure 2. It should be emphasized that the data of $\alpha_{av,i}$ vs. Δp_c are satisfactory also in the low pressures ranging from 5 to 20 kPa. The solid curve representing $\alpha_{av,i}$ vs. Δp_c is obtained from the curve fitting based on Eq. 20. It is, however, difficult to accurately determine the value of the fitting parameter p_a in Eq. 17 only from the plot of $(1 - \varepsilon_{av})$ vs. Δp_c since there is insufficient porosity data in the low pressure region available. Assuming that p_a in Eq. 17 is equal to p_{a1} in Eq. 20, it is possible to obtain the fitting curve for the data of $(1 - \varepsilon_{av})$ vs. Δp_c, as shown in Figure 3b. Neither fitting curves representing the dependence of $\alpha_{av,i}$ and $(1 - \varepsilon_{av})$ on Δp_c are linear and are concave upward especially in the low Δp_c region.

In Figure 4, a flow diagram of the algorithm is illustrated for obtaining the data of α_{av} vs. Δp_c with the aid of $(1 - \varepsilon_{av})$ vs. Δp_c data and for determining the fitting adjustable parameters in Eqs. 16 and 17 from the experimental data. First of all, $\alpha_{av,i}$ vs. Δp_c data are collected from the plots of $d\theta/dv$ vs. v based on Eqs. 10 and 19, and the parameters in Eq. 20 are determined due to the data fitting. The values of α_3, p_{a1}, and n_3 thus obtained are set as the initial values of α_2, p_a, and n_2 in Eq. 16 relating α_{av} to Δp_c, respectively. Then, the parameters, ε_2 and β_2, in Eq. 17 are determined to fit the data of $(1 - \varepsilon_{av})$ vs. Δp_c, using the value of p_a previously obtained. The data of α_{av} vs. Δp_c are revised based on Eq. 9 in which the information on m (or ε_{av}) is necessary, and then the new values of α_2, p_a, and n_2 are evaluated. Such an iterative calculation is repeated

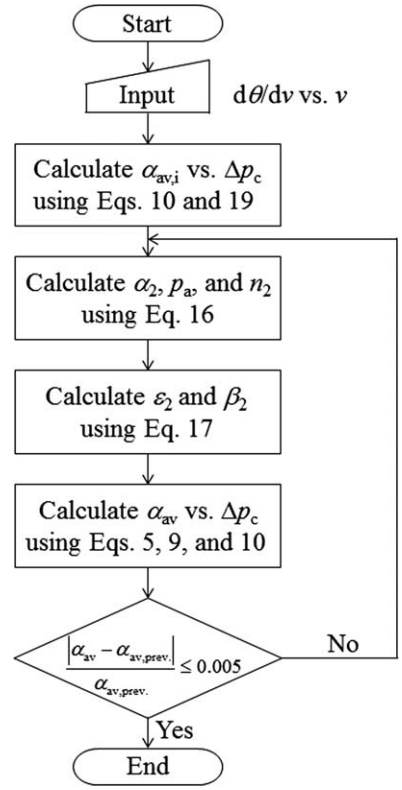

Figure 4. Flow diagram of model algorithm used in calculating fitting parameters in Eqs. 16 and 17 from experimental data.

until the datum of α_{av} corresponding to each Δp_c coincides within the range of prescribed accuracy before and after the calculation of one loop shown in the figure.

The open circles in Figure 5 show the plot of α_{av} vs. Δp_c determined based on the data in Figure 2, along with the plot of $(1 - \varepsilon_{av})$ vs. Δp_c shown in Figure 3. Comparison of Figure 5 with Figure 3 demonstrates that the difference between α_{av} and $\alpha_{av,i}$ at each Δp_c is small since the BSA concentration s in the solution is quite low. The solid curves fitted to α_{av} and $(1 - \varepsilon_{av})$ vs. Δp_c data represent the calculations obtained based on Eqs. 16 and 17, respectively. Both curves can be approximated by the straight lines in accordance with Eqs. 14 and 15 in the

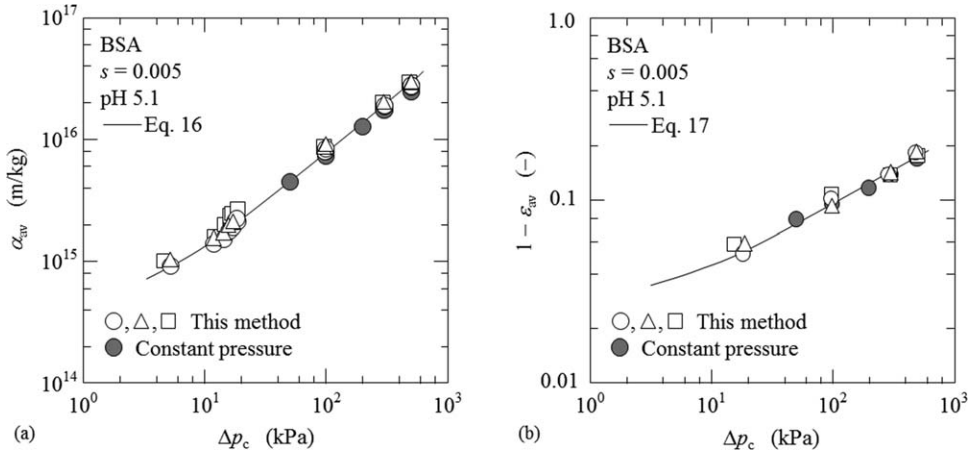

Figure 5. Pressure dependence of cake properties obtained in dead-end ultrafiltration of BSA solution with concentration of 0.005 and pH 5.1.

(a) Pressure dependence of average specific cake resistance and (b) pressure dependence of average cake solidosity.

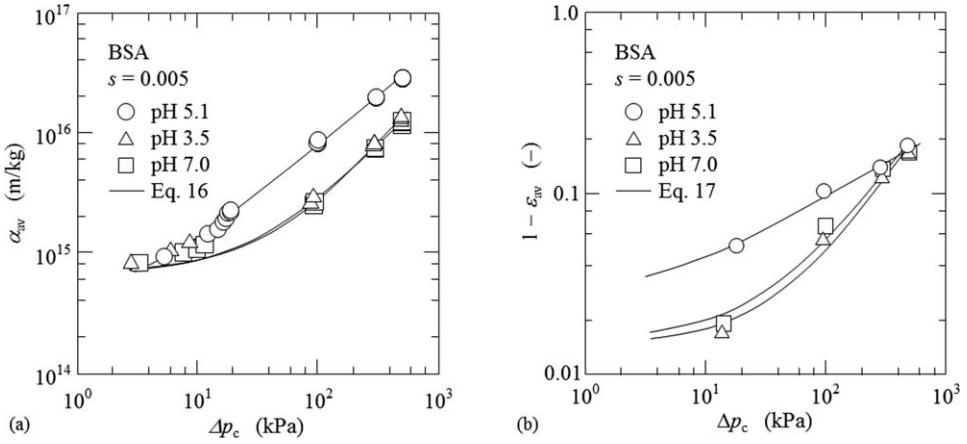

Figure 6. Effect of solution pH on cake properties obtained in dead-end ultrafiltration of BSA solution with concentration of 0.005.

(a) Pressure dependence of average specific cake resistance and (b) pressure dependence of average cake solidosity.

pressure range of more than ca. 20 kPa. To examine the deviations in the experimental data obtained by this method, Figure 5 includes the experimental data (plotted as open triangles and squares) obtained from the other two runs carried out under the same operating conditions as the open circles. The results clearly show that the test is a highly reproducible. What remains to be seen is to acquire the cake porosity data in lower Δp_c range to confirm the plausibility of the solid curve fitted to the data of $(1 - \varepsilon_{av})$ vs. Δp_c. The filled circles in the figure are the data obtained from several constant pressure filtration experiments conducted under pressure conditions ranging from 49 to as high as 490 kPa. The constant pressure filtration data are in fair agreement with the data obtained by this method, clearly indicating that the cake is readily compressed to the state corresponding to the increased pressure in response to the pressure jump in step-up pressure filtration. However, it should be emphasized that only one data point is determined from one experiment in constant pressure filtration. Therefore, several constant pressure filtration experiments are necessary to depict the curves of α_{av} and $(1 - \varepsilon_{av})$ vs. Δp_c.

Dependence of α_{av} and ε_{av} on pH and salt concentration

It is well known that the solution environment of pH and ionic strength frequently makes a profound impact on dead-end filtration behaviors of nanocolloids.[3,16,46] The effect of solution pH on the BSA cake properties is illustrated in Figure 6. The values of α_{av} are similar irrespective of pH in the relatively low-pressure range below approximately 10kPa. However, as Δp_c is increased, the curves for α_{av} at pH 3.5 and 7.0 where BSA molecules have electronic charges lie below the curve for pH 5.1 around the isoelectric point of BSA. But, the behaviors of dependence of ε_{av} on pH show a very dissimilar trend. The values of $(1 - \varepsilon_{av})$ are very similar irrespective of pH in the relatively high-pressure range above ca. 300 kPa. However, as Δp_c is decreased, the curves for $(1 - \varepsilon_{av})$ at pH 3.5 and 7.0 lie below the curve for pH 5.1. Considering that in general a loose filter cake with a high porosity has a low specific cake resistance, the results of Figure 6 seemingly look strange. A possible explanation for our experimental data is as follows. The electrostatic repulsion force between charged BSA molecules becomes more remarkable at pH 3.5 and 7.0 than at pH 5.1 because BSA molecules have positive charges at pH 3.5 and negative charges at pH 7.0. As a result, the cake porosity ε_{av} becomes higher at pH 3.5 and 7.0, largely influenced by the electrostatic repulsion force in the low Δp_c region. However, the specific cake resistance α_{av} at pH 3.5 and 7.0 is comparable with that at pH 5.1. This is because α_{av} at the same porosity becomes higher for charged molecules in

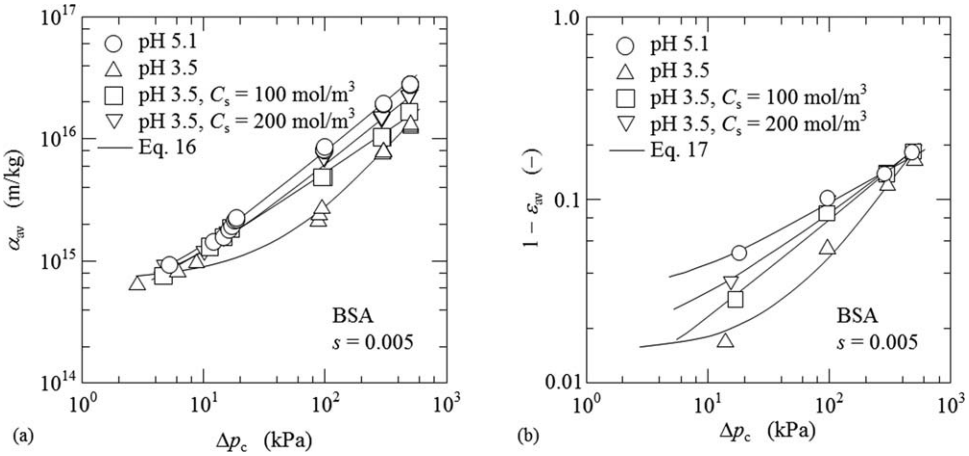

Figure 7. Effect of salt concentration on cake properties obtained in dead-end ultrafiltration of BSA solution with concentration of 0.005.

(a) Pressure dependence of average specific cake resistance and (b) pressure dependence of average cake solidosity.

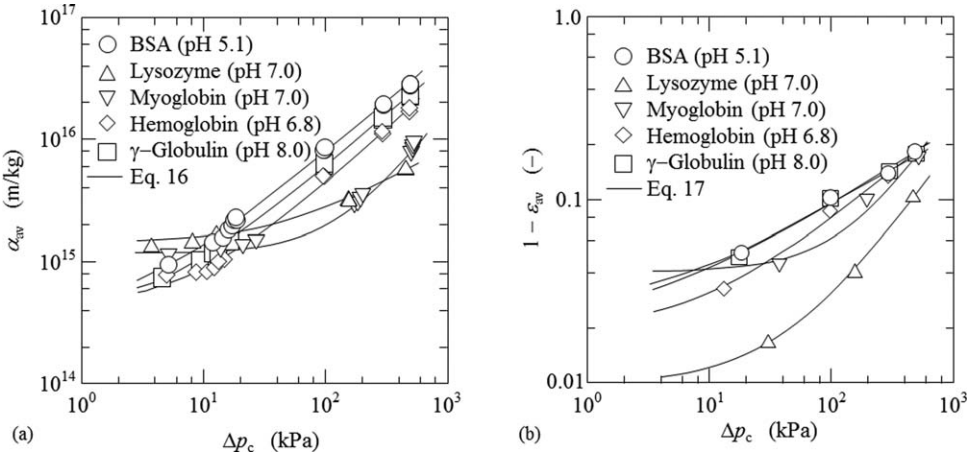

Figure 8. Cake properties obtained in dead-end ultrafiltration of several protein solutions.

(a) Pressure dependence of average specific cake resistance and (b) pressure dependence of average cake solidosity.

the relatively high porosity range, influenced by intramolecular charges, as verified by the ultracentrifugal sedimentation data of BSA solution.[16,64] In contrast, as Δp_c is increased, ε_{av} at pH 3.5 and 7.0 becomes comparable with that at pH 5.1, largely influenced by the solute compressive force overcoming the electrostatic repulsion force. In this case, α_{av} at pH 5.1 becomes higher than that at pH 3.5 and 7.0. This result suggests that the molecular size becomes smaller at pH 5.1, leading to the increase in the specific surface area of molecules. Further examination is needed to support this hypothesis and to elucidate this complex dependence of α_{av} and ε_{av} on the solution pH.

The existence of salt in the solution strongly affects the charge of macromolecules and reduces the electrical repulsion between charged macromolecules due to a less extensive diffuse double layer as discussed elsewhere.[3] The pressure dependence of the cake properties for different NaCl concentrations is illustrated in Figure 7. As the NaCl concentration C_s is increased, the plots of α_{av} and $(1 - \varepsilon_{av})$ vs. Δp_c at pH 3.5 approach those around the isoelectric point where the electrical charges are absent. This result is brought about by the charge-shielding between BSA molecules caused by the existence of salts.

Cake properties of various nanocolloids

The pressure dependence of both α_{av} and ε_{av} over a wide pressure range can be simultaneously evaluated from only one experiment by conducting the step-up pressure filtration, using a filter with a single-stage reduction in the filtration area developed in this research. Thus, it is possible to determine the cake properties for a variety of test colloids much more easily than ever before. Figure 8 illustrates the dependence of α_{av} and $(1 - \varepsilon_{av})$ on Δp_c for filter cakes formed in dead-end ultrafiltration of several protein solutions, where the values of the solution pH tested are noted in brackets. The solid curves are the calculations fitted to the experimental data by using Eqs. 16 and 17. In the low Δp_c region where the solute compressive pressure is insignificant, α_{av} generally increases with decreasing molecular weight of proteins. While both α_{av} and $(1 - \varepsilon_{av})$ increases with the increase in Δp_c, the changes exhibit the complex behaviors probably depending on the charge and deformability of proteins.

Figure 9 shows the pressure dependence of α_{av} and $(1 - \varepsilon_{av})$ for nanocolloids of silica sol with the mean specific surface area sizes d_s ranging from 4.8 to 99.7 nm. Both α_{av} and ε_{av} increase with decreasing particle size. Therefore, although the decrease in the particle size leads to low filterability, the structure of the cake formed becomes loose and wet.

Effect of solution concentration on filtration behaviors

When the solution is dilute, the filtration rate in dead-end filtration can be well evaluated from Eqs. 10 and 11 using the

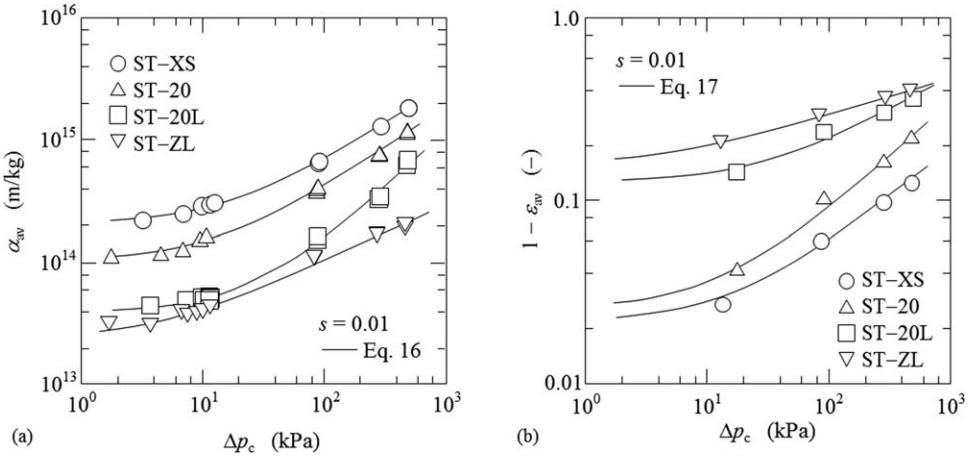

Figure 9. Cake properties obtained in dead-end ultrafiltration of nanosilica sol.

(a) Pressure dependence of average specific cake resistance and (b) pressure dependence of average cake solidosity.

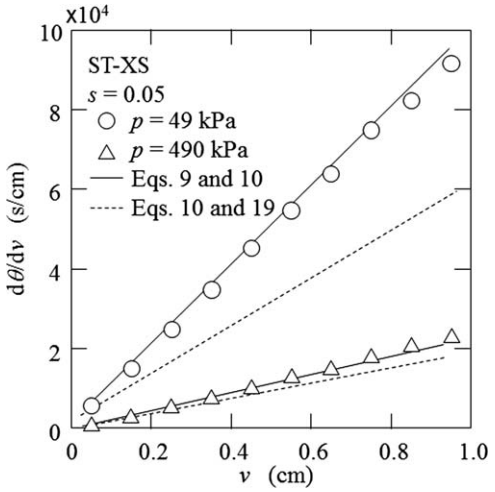

Figure 10. Relation between reciprocal filtration rate and filtrate volume per unit effective membrane area in constant pressure dead-end ultrafiltration of nanosilica sol with concentration of 0.05.

relation between α_{av} and Δp_c without information about the relation between $(1 - \varepsilon_{av})$ and Δp_c. However, as the solution concentration becomes high, the difference between α_{av} and $\alpha_{av,i}$ becomes measurable and Eqs. 9 and 10 have to be employed to evaluate the temporal flux decline behaviors in dead-end filtration with the aid of the relation between $(1 - \varepsilon_{av})$ and Δp_c. In Figure 10, the plots of $d\theta/dv$ vs. v are illustrated for constant pressure dead-end filtration conducted at different pressures of 49 and 490 kPa using nanosilica sol with the relatively high solution concentration ($s = 0.05$) compared with the concentration ($s = 0.01$) of the solution tested in Figure 9. Both plots show linear relationships with different slopes in accordance with Eq. 7 since α_{av} and ε_{av} (i.e., m) remain unchanged over the entire period of filtration under constant pressure conditions. The dotted lines are the predictions obtained from Eqs. 10 and 19 with the data of $\alpha_{av,i}$ vs. Δp_c obtained using nanosilica sol with the concentration s of 0.01. The solid lines are the calculations obtained from Eqs. 9 and 10 with the data of α_{av} and $(1 - \varepsilon_{av})$ vs. Δp_c shown in Figure 9 obtained using nanosilica sol with s of 0.01. The calculations based on Eqs. 10 and 19 seriously overestimate the filtration rate in constant pressure dead-end filtration particularly in the low pressure range. Therefore, it is essential to rigorously take the cake porosity into account in accurate evaluation of the flux decline behaviors in dead-end filtration of relatively thick colloids.

Figure 11 shows $d\theta/dv$ vs. v and $dv/d\theta$ vs. θ relations in constant pressure dead-end filtration of nanosilica sol with concentrations s ranging from 0.03 to 0.10 and applied pressures p ranging from 49 to 490 kPa. The solid lines are the calculations obtained from Eqs. 9 and 10 by using the data shown in Figure 9 and are in excellent agreement with the experimental data over the entire concentration and pressure range. It should be emphasized that the flux decline behaviors under a wide variety of concentration and pressure conditions can be evaluated from the data acquired by conducting only one filtration experiment developed in this research.

Conclusion

Making use of the filtration behavior under each constant pressure condition and the decrease in the cake thickness caused by the pressure rise, the pressure dependences of not only the average specific cake resistance but also the average cake porosity of highly compressible filter cake were evaluated using only one run of the step-up pressure dead-end filtration test by using a filer with a single-stage reduction in the filtration area. The method was applied to the determination of cake properties of a variety of nanocolloids, and its relevance was substantiated through the comparison with cake properties obtained from several constant pressure filtration tests carried out under various pressures. It was found that constant pressure filtration data obtained under various pressures and concentrations can be well evaluated based on the pressure dependences of the average specific cake resistance and

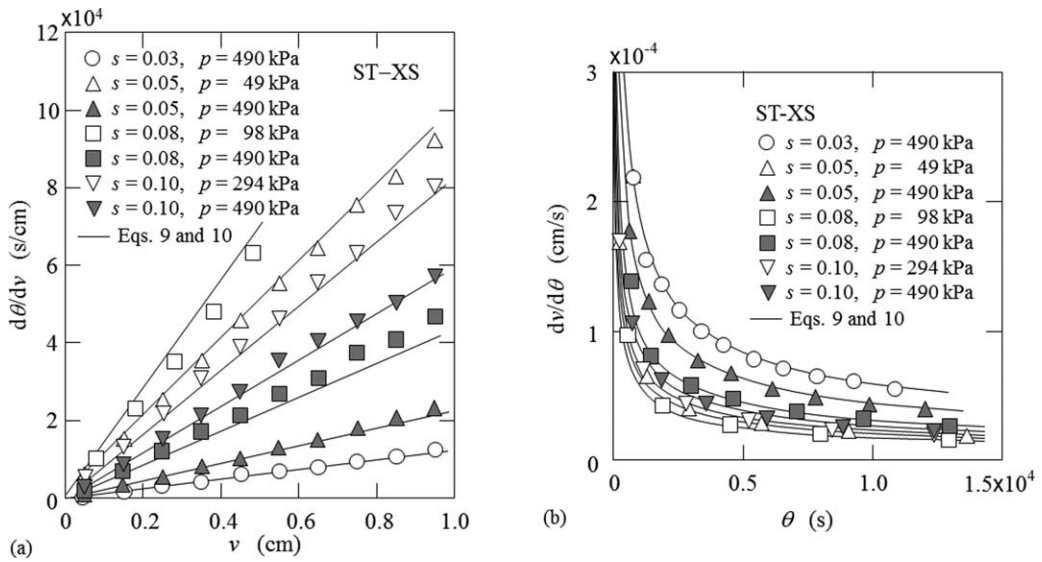

Figure 11. Evaluation of flux decline behaviors in constant pressure dead-end ultrafiltration of nanosilica sol conducted under a variety of solution concentration and applied filtration pressure conditions.

(a) Relation between reciprocal filtration rate and filtrate volume per unit effective membrane area and (b) relation between filtration rate and filtration time.

average cake porosity obtained from this method. We believe that the method developed in this research may be readily applicable also in the determination of properties of compressible filter cake formed in cake filtration of particulate suspension.

Acknowledgments

This work was supported in part by the Grants-in-Aid for Scientific Research from The Ministry of Education, Culture, Sports, Science and Technology, Japan and from The Ministry of the Environment, Japan. The authors acknowledge with sincere gratitude the financial support leading to the publication of this article.

Notation

C_s = NaCl concentration in solution, mol/m^3
d_s = mean specific surface area size of nanoparticles, m
$(d\theta/dv)_m$ = reciprocal filtration rate at start of filtration, s/m
h = distance from membrane surface to position where filtration area is reduced, m
L = cake thickness, m
m = ratio of mass of wet to mass of dry cake
n_1 = empirical constant in Eq. 14
n_2 = empirical constant in Eq. 16
n_3 = empirical constant in Eq. 20
p = applied filtration pressure, Pa
p_a = empirical constant in Eqs. 16 and 17, Pa
p_{a1} = empirical constant in Eq. 20, Pa
p_i = applied filtration pressure at the i-th stage in step-up pressure filtration, Pa
p_L = local hydraulic pressure, Pa
p_s = local solute compressive pressure, Pa
R_m = membrane resistance, m^{-1}
s = mass fraction of solutes in colloid
u = apparent liquid velocity relative to solids in cake at distance ω from membrane, m/s
u_1 = filtration rate, m/s
v = cumulative filtrate volume per unit effective membrane area, m
v_c = cumulative filtrate volume per unit effective membrane area at transition point when applied filtration pressure is increased stepwise, m
$v_{c,i}$ = cumulative filtrate volume per unit effective membrane area at transition point when applied filtration pressure is increased to p_{i+1} stepwise, m
v_t = cumulative filtrate volume per unit effective membrane area collected until filter cake surface reaches reduced surface, m
$v_{t,i}$ = cumulative filtrate volume per unit effective membrane area collected until filter cake surface reaches reduced surface for the i-th time, m

Greek letters

α = local specific cake resistance, m/kg
α_{av} = average specific cake resistance, m/kg
$\alpha_{av,i}$ = infinite average specific cake resistance defined by Eq. 18, m/kg
α_1 = empirical constant in Eq. 14, kg$^{-n_1-1}$ m$^{1+n_1}$ s^{2n_1}
α_2 = empirical constant in Eq. 16, m/kg
α_3 = empirical constant in Eq. 20, m/kg
β_1 = empirical constant in Eq. 15
β_2 = empirical constant in Eq. 17
Δp_c = pressure drop across filter cake, Pa
Δp_m = pressure drop across membrane, Pa
ε = local porosity
ε_{av} = average porosity of filter cake
ε_1 = empirical constant in Eq. 15
ε_2 = empirical constant in Eq. 17
θ = filtration time, s
θ_i = filtration time at end of the i-th stage in step-up pressure filtration, s
μ = viscosity of filtrate, Pa s
Π = osmotic pressure, Pa
ρ = density of filtrate, kg/m^3
ρ_s = density of solutes, kg/m^3
ω = net solute volume per unit membrane area lying from membrane up to an arbitrary position in filter cake, m
ω_0 = net solute volume of entire filter cake per unit membrane area, m

Literature Cited

1. Reihanian H, Robertson CR, Michaels AS. Mechanism of polarization and fouling of ultrafiltration membranes by proteins. *J Membr Sci*. 1983;16:237–258.
2. Chudacek MW, Fane AG. The dynamics of polarization in unstirred and stirred ultrafiltration. *J Membr Sci*. 1984;21:145–160.
3. Iritani E, Nakatsuka S, Aoki H, Murase T. Effect of solution environment on unstirred dead-end ultrafiltration characteristics of proteinaceous solutions. *J Chem Eng Jpn*. 1991;24:177–183.
4. Nakakura H, Yamashita A, Sambuichi M, Osasa K. Electrical conductivity measurement of filter cake in dead-end ultrafiltration of protein solution. *J Chem Eng Jpn*. 1997;30:1020–1025.
5. Mohammadi T, Kohpeyma A, Sadrzadeh M. Mathematical modeling of flux decline in ultrafiltration. *Desalination*. 2005;184:367–375.
6. Thekkedath A, Naceur WM, Kecili K, Sbai M, Elane A, Auret L, Suty H, Machinal C, Pontié M. Macroscopic and microscopic characterization of a cellulosic ultrafiltration (UF) membrane fouled by a humic acid cake deposit: first step for intensification of reverse osmosis (RO) pre-treatments. *C R Chim*. 2007;10:803–812.
7. Sarkar B. A combined complete pore blocking and cake filtration model during ultrafiltration of polysaccharide in a batch cell. *J Food Eng*. 2013;116:333–343.
8. Salinas-Rodriguez SG, Amy GL, Schippers JC, Kennedy MD. The Modified Fouling Index Ultrafiltration constant flux for assessing particulate/colloidal fouling of RO systems. *Desalination*. 2015;365:79–91.
9. Iritani E, Itano Y, Murase T. Ultrafiltration of proteinaceous solutions by use of dynamic membranes formed by body-feed method. *Membrane*. 1992;17:203–206.
10. Iritani E. A review on modeling of pore-blocking behaviors of membranes during pressurized membrane filtration. *Dry Technol*. 2013;31:146–162.
11. Fane AG, Fell CJD, Suki A. The effect of pH and ionic environment on the ultrafiltration of protein solutions with retentive membranes. *J Membr Sci*. 1983;16:195–210.
12. Iritani E, Tachi S, Murase T. Influence of protein adsorption on flow resistance of microfiltration membrane. *Colloids Surf A: Physicochem Eng Aspects*. 1994;89:15–22.
13. Kimura S, Sourirajan S. Analysis of data in reverse osmosis with porous cellulose acetate membranes used. *AIChE J*. 1967;13:497–503.
14. Vilker VL, Colton CK, Smith KA. Concentration polarization in protein ultrafiltration. *AIChE J*. 1981;27:632–645.
15. Iritani E, Hattori K, Murase T. Analysis of dead-end filtration based on ultracentrifugation method. *J Membr Sci*. 1993;81:1–13.
16. Iritani E, Hattori K, Murase T. Evaluation of dead-end ultrafiltration properties by ultracentrifugation method. *J Chem Eng Jpn*. 1994;27:357–362.
17. Iritani E, Mukai Y, Hagihara E. Measurements and evaluation of concentration distributions in filter cake formed in dead-end ultrafiltration of protein solutions. *Chem Eng Sci*. 2002;57:53–62.
18. Lodge B, Judd SJ, Smith AJ. Characterisation of dead-end ultrafiltration of biotreated domestic wastewater. *J Membr Sci*. 2004;231:91–98.
19. Tiller FM, Cooper HR. The role of porosity in filtration: IV. Constant pressure filtration. *AIChE J*. 1960;6:595–601.
20. Tiller FM, Cooper H. The role of porosity in filtration: Part V. Porosity variation in filter cakes. *AIChE J*. 1962;8:445–449.
21. Mendret J, Guigui C, Schmitz P, Cabassud C. In situ dynamic characterization of fouling under different pressure conditions during dead-end filtration: compressibility properties of particle cakes. *J Membr Sci*. 2009;333:20–29.
22. Loginov M, Citeau M, Lebovka N, Vorobiev E. Evaluation of low-pressure compressibility and permeability of bentonite sediment from centrifugal consolidation data. *Sep Purif Technol*. 2012;92:168–173.
23. Tiller FM, Green TC. Role of porosity in filtration IX Skin effect with highly compressible materials. *AIChE J*. 1973;19:1266–1269.

24. Tiller FM, Yeh CS. Compressibility of particulate structures in relation to thickening, filtration, and expression—a review. *Sep Sci Technol*. 1987;22:1037–1063.
25. Jönsson K, Jönsson B. Fluid flow in compressible porous media: I: steady-state conditions. *AIChE J*. 1992;38:1340–1348.
26. Sørensen PB, Hansen JA. Extreme solid compressibility in biological sludge dewatering. *Water Sci Technol*. 1993;28:133–143.
27. Shen C, Russel WB, Auzerais FM. Colloidal gel filtration: experiment and theory. *AIChE J*. 1994;40:1876–1891.
28. Landman KA, White LR, Eberl M. Pressure filtration of flocculated suspensions. *AIChE J*. 1995;41:1687–1700.
29. Lee DJ, Ju SP, Kwon JH, Tiller FM. Filtration of highly compactible filter cake: variable internal flow rate. *AIChE J*. 2000;46:110–118.
30. Lu WM, Tung KL, Hung SM, Shiau JS, Hwang KJ. Constant pressure filtration of mono-dispersed deformable particle slurry. *Sep Sci Technol*. 2001;36:2355–2383.
31. Bouchoux A, Qu P, Bacchin P, Gésan-Guiziou G. A general approach for predicting the filtration of soft and permeable colloids: the milk example. *Langmuir*. 2014;30:22–34.
32. Shirato M, Sambuichi M, Kato H, Aragaki T. Internal flow mechanism in filter cakes. *AIChE J*. 1969;15:405–409.
33. Shirato M, Murase T, Iritani E, Tiller FM, Alciatore AF. Filtration in the chemical process industry. In: Matteson MJ, Orr C, editors. *Filtration: Principles and Practices*. New York: Marcel Dekker, Inc., 1987:299–420.
34. Olivier J, Vaxelaire J, Vorobiev E. Modelling of cake filtration: an overview. *Sep Sci Technol*. 2007;42:1667–1700.
35. Tarleton ES, Wakeman RJ. *Solid/Liquid Separation: Equipment Selection and Process Design*. Oxford: Elsevier, Ltd., 2007.
36. Shirato M, Aragaki T, Mori R, Sawamoto K. Predictions of constant pressure and constant rate filtrations based upon an approximate correction for side wall friction in compression permeability cell data. *J Chem Eng Jpn*. 1968;1:86–90.
37. Tiller FM. The role of porosity in filtration, Part 3: variable-pressure-variable-rate filtration. *AIChE J*. 1958;4:170–174.
38. Murase T, Iritani E, Cho JH, Shirato M. Determination of filtration characteristics based upon filtration tests under step-up pressure conditions. *J Chem Eng Jpn*. 1989;22:373–378.
39. Chen W. Analysis of compressible suspensions for an effective filtration and deliquoring. *Drying Technol*. 2006;24:1251–1256.
40. Iritani E, Katagiri N, Kanetake S. Determination of cake filtration characteristics of dilute suspension of bentonite from various filtration tests. *Sep Purif Technol*. 2012;92:143–151.
41. Iritani E, Katagiri N, Tsukamoto M, Hwang KJ. Determination of cake properties in ultrafiltration of nano-colloids based on single step-up pressure filtration test. *AIChE J*. 2014;60:289–299.
42. Okamura S, Shirato M. Liquid pressure distribution within cakes in the constant pressure filtration. *Kagaku Kogaku*. 1955;19:104–110.
43. Shirato M, Aragaki T, Ichimura K, Ootsuji N. Porosity variation in filter cake under constant-pressure filtration. *J Chem Eng Jpn*. 1971; 4:172–177.
44. Murase T, Iritani E, Cho JH, Nakanomori S, Shirato M. Determination of filtration characteristics due to sudden reduction in filtration area of filter cake surface. *J Chem Eng Jpn*. 1987;20:246–251.
45. Murase T, Iritani E, Cho JH, Shirato M. Determination of filtration characteristics of power-law non-Newtonian fluids-solids mixtures under constant-pressure conditions. *J Chem Eng Jpn*. 1989;22:65–71.
46. Iritani E, Mukai Y, Murase T. Properties of filter cake in dead-end ultrafiltration of binary protein mixtures with retentive membranes. *Trans IChemE A: Chem Eng Res Des*. 1995;73:551–558.
47. Iritani E, Nagaoka H, Katagiri N. Determination of filtration characteristics of yeast suspension based upon multistage reduction in cake surface area under step-up pressure conditions. *Sep Purif Technol*. 2008;63:379–385.
48. Iritani E, Katagiri N, Nakajima R, Hwang KJ, Cheng TW. Cake properties of nanocolloid evaluated by variable pressure filtration associated with reduction in cake surface area. *AIChE J*. 2014;60: 3869–3877.
49. Encyclopaedia Chimica Editing Committee, editor. *Encyclopaedia Chimica, Vol. IX*. Tokyo: Kyoritu Shuppan Co., Ltd., 1964.
50. Japanese Biochemical Society, editor. *Biochemical Data Book, Vol. I*. Tokyo: Tokyo Kagaku-Dojin Publishing Co., Inc., 1979.
51. Van den Berg GB, Smolders CA. Flux decline in ultrafiltration processes. *Desalination*. 1990;77:101–133.
52. DeMoll E, Cox DJ, Daniel E, Riggs AF. Apparent specific volume of human hemoglobin: effect of ligand state and contribution of heme. *Anal Biochem*. 2007;363:196–203.
53. Ruth BF. Studies in filtration. III. Derivation of general filtration equations. *Ind Eng Chem*. 1935;27:708–723.
54. Shirato M, Aragaki T, Iritani E. Analysis of constant pressure filtration of power-law non-Newtonian fluids. *J Chem Eng Jpn*. 1980;13: 61–66.
55. Iritani E, Katagiri N, Takaishi Y, Kanetake S. Determination of pressure dependence of permeability characteristics from single constant pressure filtration test. *J Chem Eng Jpn*. 2011;44:14–23.
56. Jönsson AS, Jönsson B. Ultrafiltration of colloidal dispersions—a theoretical model of the concentration polarization phenomena. *J Colloid Interface Sci*. 1996;180:504–518.
57. Elimelech M, Bhattacharjee S. A novel approach for modeling concentration polarization in crossflow membrane filtration based on the equivalence of osmotic pressure model and filtration theory. *J Membr Sci*. 1998;145:223–241.
58. Tiller FM, Shirato M. The role of porosity in filtration: VI. New definition of filtration resistance. *AIChE J*. 1964;10:61–67.
59. Tiller FM, Crump JR, Ville F. A revised approach to the theory of cake filtration. *Proceedings of International Symposium on Fine Particles Processing*, *Vol. 2*. Las Vegas, USA. 1980:1549–1582.
60. Sperry DR. Note and correspondence: a study of the fundamental laws of filtration using plant-scale equipment. *Ind Eng Chem*. 1921; 13:1163–1164.
61. Tiller FM, Lue WF. Basic data fitting in filtration. *J Chin Inst Chem Eng*. 1980;11:61–70.
62. Cao DQ, Iritani E, Katagiri N. Evaluation of filtration properties in membrane filtration of O/W emulsion based on upward dead-end constant pressure filtration. *Kagaku Kogaku Ronbunshu*. 2012;38: 378–383.
63. Cao DQ, Iritani E, Katagiri N. Properties of filter cake during dead-end microfiltration of O/W emulsion. *J Chem Eng Jpn*. 2013;46: 593–600.
64. Van Holde KE. Sedimentation analysis of proteins. In: Neurath H, Hill RL, editors. *The Proteins*, 3rd ed., *Vol*. I. New York: Academic Press, 1975:235–238.

Manuscript received Apr. 21, 2015, and revision received July 15, 2015.